Chapter 29
Fast PPP Ambiguity Resolution Using a Sparse Regional Reference Network

Yihe Li and Yang Gao

Abstract Precise point positioning real-time kinematic (PPP-RTK) can achieve fast ambiguity resolution and precise positioning with the satellite fractional cycle biases (FCBs) and atmospheric correction derived from a dense regional reference network. However, the interpolated atmospheric corrections based on a sparse reference network with inter-station distances of more than 100 km are not precise enough to facilitate reliable PPP ambiguity resolution. In this contribution, a new method is proposed for fast PPP ambiguity resolution within a sparse regional reference network. First, code biases, FCBs, biased ionospheric and tropospheric delays at the reference stations are estimated with known positioning using the regional sparse reference network data. Then, the biased ionospheric and tropospheric corrections at a user station are generated using a distance-based linear interpolation of the ionospheric and tropospheric delays available at the reference stations. To strengthen the observation model, the interpolated ionospheric and tropospheric delays derived from the sparse network are all considered as pseudo-observations with a given variance-covariance matrix which will be adaptively estimated according to the reference network density to describe the level of the constraint strength. To get a realistic constraint variance, atmospheric constraint variance is estimated with a certain window length. By a proper tuning of the variance-covariance matrix applied for the atmospheric pseudo-observations, the method can adapt any scale of the regional reference network. The ambiguity fixing performance and the resulted position accuracy are assessed with medium and large reference networks. The validation confirms that the new strategy can fix ambiguity within 1 min for a medium network and within 7 min for a larger network while provide centimeter-level positioning solution ambiguity with 20.8 s for a medium network and within 71.9 s for a larger network.

Y. Li (✉) · Y. Gao
Department of Geomatics Engineering, The University of Calgary, Calgary, Canada
e-mail: yihli@ucalgary.ca

29.1 Introduction

Precise point positioning (PPP) is the technique to derive centimeter-level positioning accuracy using a single receiver and the precise clock and orbit products from International GNSS Service (IGS) [1]. It has drawn the increasing research attentions over the past years and has been applied to various applications, for instance, estimating the tropospheric delays for meteorology, monitoring the earthquakes and tsunamis, precision agriculture etc. [2–4]. Typically, dual-frequency code and phase measurements are used to form linear ionosphere-free observations (L3) for removing the first-order ionosphere effects. Apart from the position coordinates, ambiguities, receiver clock bias and troposphere zenith wet delay (ZWD) parameters are also estimated in PPP solution. Integer ambiguity fixing has the potential to significantly shorten the time-to-fixed- solution (TTFS) and improve the PPP positioning accuracy when fractional cycle biases (FCBs) are available to recover the integer feature of integer ambiguities [5–7]. But this approach would still require approximate 20–30 min to reliably fix the integer ambiguities.

The ionosphere and troposphere are considered as two key dominating error sources limiting the capability of carrier phase fast ambiguity resolution (AR) and the positioning precision [8]. Due to lack of precise ionospheric model, the positioning model is based on the L3 observations in which both wide-lane (WL) and narrow-lane (NL) ambiguities are to be fixed. The large noise of the range observations (which are definitely needed for WL ambiguity fixing) and the short NL wavelength result in a long initialization time for ambiguity-fixing. Besides, once the tropospheric ZWD parameter is estimated along with coordinate parameters, the model is seriously ill-conditioned due to its strong correlation with the height parameter as recognized by Dodson et al. [9]. Thus, it cannot be precisely solved without long period observation accumulation. In general, the residual tropospheric delays are typically modeled as a first-order Gauss-Markov random walk process, and a filtering technique, such as Kalman filtering, is often used. In a static scenario, the results from Tralli and Lichten [10] suggested that a few minutes of GPS observations provide sufficient strength to resolve centimeter-level zenith delay fluctuations.

To reliably resolve the ambiguities, both of the ionospheric and tropospheric errors have to be kept as small as possible. Shi [11] proposed a troposphere constraint method to improve the PPP ambiguity resolution as well as height solution by using the station-based IGS troposphere ZWD product. This method essentially specifies the correlation between the RZTD and three position components. However, the external troposphere corrections are chosen as the station-based IGS troposphere ZWD product which is probably not the optimal choice in practice. Ge et al. [12] proposed a network real-time kinematic positioning (NRTK) strategy

using pre-fit undifferenced observation residuals of the reference network with linear combination to remove biases and recover the integer feature of the ambiguities at user stations. Li et al. [13] retrieved atmospheric delays as corrections from data derived by a regional dense network to accelerate convergence. However, both of the above two methods ignore the retrieved atmospheric delay errors and can be only suitable for networks with short inter-station distances. In order to achieve fast or instantaneous AR with medium or long inter-station distances, both ionospheric and tropospheric errors have to be considered after a priori corrections. Therefore, the ionosphere-weighted model in which the ionospheric delays are treated stochastically instead of deterministically [14–19] is introduced into PPP AR. Its popularity stems from improving the model strength through adding prior stochastic information of ionospheric delays in term of zero-valued ionospheric pseudo-observations and stochastic model. Moreover, the relative variation of the ionosphere delay between consecutive epochs is also taken into account in term of pseudo-observations. Li [20] improved PPP ambiguity resolution performance considering the ionospheric characteristics by adding spatial and temporal constraints after correcting the slant delay using the IGS Global-Ionospheric-Maps (GIMs). As a result, the convergence time can be reduced by 30 %.

The accuracy of the interpolated atmospheric corrections at the user station depends on the density of the regional reference network. For a sparse reference network with the inter-station distance more than 100 km, the interpolated atmospheric corrections could be not precise enough to facilitate reliable PPP ambiguity resolution. The choice of the ionospheric constraint variance should correspond to the expected statistical behaviour of the noise of the ionospheric delays. In this contribution, we will propose a new method for fast PPP ambiguity resolution using the corrections of a sparse regional reference network. To get a realistic constraint variance, atmospheric constraint variance is adaptively estimated according to the reference network density with a certain window length. The performance of our proposed method is demonstrated by using both networks with medium and long inter-station distances. The rest of the paper is organized as follows. Our new method is presented in Sect. 29.2, two experiments are demonstrated in Sect. 29.3, and conclusions are given out in Sect. 29.4.

29.2 Regional Augmentation PPP with Atmospheric Constraint

29.2.1 Augmentation Information from Regional Reference Network

Undifferenced GPS code and phase observations on frequencies L1 and L2 are denoted as

$$
\begin{cases}
P_1 = \rho + d_{orb} + c(dt^r - dt^s) + T + I + b_{P_1}^r - b_{P_1}^s + \varepsilon_{P_1} \\
P_2 = \rho + d_{orb} + c(dt^r - dt^s) + T + \frac{f_1^2}{f_2^2}I + b_{P_2}^r - b_{P_2}^s + \varepsilon_{P_2} \\
L_1 = \rho + d_{orb} + c(dt^r - dt^s) + T - I - \lambda_1 N_1 + b_{L_1}^r - b_{L_1}^s + \varepsilon_{L_1} \\
L_2 = \rho + d_{orb} + c(dt^r - dt^s) + T - \frac{f_1^2}{f_2^2}I - \lambda_2 N_2 + b_{L_2}^r - b_{L_2}^s + \varepsilon_{L_2}
\end{cases}
\tag{29.1}
$$

where, $i = 1, 2$ denotes the L1 and L2 frequencies, P_i and L_i are the raw code and phase measurements (m), ρ is the geometric distance between receiver and satellite (m), d_{orb} is the satellite orbit error (m), c is the speed of light in vacuum (m/s); dt^r and dt^s are the common receiver and satellite clock biases (s), T is the tropospheric delay (m), I is the first-order ionospheric delay, f_i is the frequency (H_z), λ_i is the carrier phase wavelength (m), N_i is the integer ambiguity (cycle); $b_{P_i}^r$ and $b_{P_i}^s$ are the observable-dependent receiver and satellite code biases (m); $b_{L_i}^r$ and $b_{L_i}^s$ are the observable-dependent receiver and satellite FCB (m); ε_{P_i} and ε_{L_i} are the code and phase observation errors including multipath noises (m).

Since the coordinates of all stations of a regional reference network and precise satellite orbits are known, the dry component of tropospheric delays can be corrected with a priori model, and the remaining ZWD delay is modeled as piece-wise constants, the WL and NL ambiguities (N_{NL} and N_{WL})can be resolved in a few minutes. Once the WL and NL ambiguities are fixed on the reference stations, the L1 and L2 integer ambiguities can be easily derived, and the ZWD delay, the satellite and receiver clock biases (dt^s and dt^r) as well as the FCBs ($b_{L_3}^s$ and $b_{L_3}^r$) and code biases ($b_{P_3}^s$ and $b_{P_3}^r$) can be computed accurately using L3 and P3 observation equations as follows

$$
P_3 = \rho + d_{orb} + \left(cdt^r + b_{P_3}^r\right) - \left(dt^s + b_{P_3}^s\right) + T + \varepsilon_{P_3}
$$
$$
L_3 = \rho + d_{orb} + \left(cdt^r + b_{L_3}^r\right) - \left(dt^s + b_{L_3}^s\right) + T - \lambda_3(17N_{NL} + 60N_{WL}) + \varepsilon_{L_3}
\tag{29.2}
$$

The FCBs and code biases w.r.t L3 observation are as follows,

$$
b_{L_3}^s = \frac{f_1^2}{f_1^2 - f_2^2}b_{L_1}^s - \frac{f_2^2}{f_1^2 - f_2^2}b_{L_2}^s, \qquad b_{L_3}^r = \frac{f_1^2}{f_1^2 - f_2^2}b_{L_1}^r - \frac{f_2^2}{f_1^2 - f_2^2}b_{L_2}^r
$$
$$
b_{P_3}^s = \frac{f_1^2}{f_1^2 - f_2^2}b_{P_1}^s - \frac{f_2^2}{f_1^2 - f_2^2}b_{P_2}^s, \qquad b_{P_3}^r = \frac{f_1^2}{f_1^2 - f_2^2}b_{P_1}^r - \frac{f_2^2}{f_1^2 - f_2^2}b_{P_2}^r
\tag{29.3}
$$

Therefore, the undifferenced observation equation shown in Eq. (29.1) corrected by code biases and FCBs shown in Eq. (29.3) is expressed as

$$
\begin{cases}
P_1 - b_{P_3}^r + b_{P_3}^s = \rho + d_{orb} + c(dt^r - dt^s) + T + I + b_{P_1}^r - b_{P_1}^s - b_{P_3}^r + b_{P_3}^s + \varepsilon_{P_1} \\
P_2 - b_{P_3}^r + b_{P_3}^s = \rho + d_{orb} + c(dt^r - dt^s) + T + \frac{f_1^2}{f_2^2} I + b_{P_2}^r - b_{P_2}^s - b_{P_3}^r + b_{P_3}^s + \varepsilon_{P_2} \\
L_1 - b_{L_3}^r + b_{L_3}^s = \rho + d_{orb} + c(dt^r - dt^s) + T - I - \lambda_1 N_1 + b_{L_1}^r - b_{L_1}^s - b_{L_3}^r + b_{L_3}^s + \varepsilon_{L_1} \\
L_2 - b_{L_3}^r + b_{L_3}^s = \rho + d_{orb} + c(dt^r - dt^s) + T - \frac{f_1^2}{f_2^2} I - \lambda_2 N_2 + b_{L_2}^r - b_{L_2}^s - b_{L_3}^r + b_{L_3}^s + \varepsilon_{L_2}
\end{cases}
\tag{29.4}
$$

Moving all known quantities in Eq. (29.4) to the right of equation, the term including the ionospheric delay and combination of FCBs and code biases are then derived straightforwardly as follows

$$
\begin{cases}
I + \frac{f_2^2}{f_1^2 - f_2^2} \left(b_{P_1}^s - b_{P_2}^s - b_{P_1}^r + b_{P_2}^r \right) = P_1 - \rho - c(dt^r - dt^s) - T - b_{P_3}^r + b_{P_3}^s + \varepsilon_{P_1} \\
\frac{f_1^2}{f_2^2} \left(I + \frac{f_2^2}{f_1^2 - f_2^2} \left(b_{P_1}^s - b_{P_2}^s - b_{P_1}^r + b_{P_2}^r \right) \right) = P_2 - \rho - c(dt^r - dt^s) - T - b_{P_3}^r + b_{P_3}^s + \varepsilon_{P_2} \\
I - \frac{f_2^2}{f_1^2 - f_2^2} \left(b_{L_1}^s - b_{L_2}^s - b_{L_1}^r + b_{L_2}^r \right) = \rho + c(dt^r - dt^s) + T - \lambda_1 N_1 - L_1 + b_{L_3}^r - b_{L_3}^s + \varepsilon_{L_1} \\
\frac{f_1^2}{f_2^2} \left(I - \frac{f_2^2}{f_1^2 - f_2^2} \left(b_{L_1}^s - b_{L_2}^s - b_{L_1}^r + b_{L_2}^r \right) \right) = \rho + c(dt^r - dt^s) + T - \lambda_2 N_2 - L_2 + b_{L_3}^r - b_{L_3}^s + \varepsilon_{L_2}
\end{cases}
\tag{29.5}
$$

For simplification, we call the term including the ionospheric delay and combination of phase and code biases code and phase biased ionospheric delays I_P^b and I_L^b which are derived from the either P1 or P2 code and L1 or L2 phase observations and can be written as

$$
\begin{cases}
I_P^b = I + \frac{f_2^2}{f_1^2 - f_2^2} \left(b_{P_1}^s - b_{P_2}^s - b_{P_1}^r + b_{P_2}^r \right) \\
I_L^b = I - \frac{f_2^2}{f_1^2 - f_2^2} \left(b_{L_1}^s - b_{L_2}^s - b_{L_1}^r + b_{L_2}^r \right)
\end{cases}
\tag{29.6}
$$

In practice, the I_P^b derived from P1 or P2 observations are respectively used for correcting the P1 or P2 observations at user station. The I_L^b derived from L1 or L2 observations are respectively used for correcting the L1 or L2 observations at user station.

As a summary, the augmentation information provided by reference stations are biased ionospheric delays, tropospheric ZWD, the satellite clock, as well as and code biases and FCB corrections, which will be used by user station for carrying out PPP solution.

29.2.2 Interpolation of Ionospheric and Tropospheric Corrections

The reference-station-specific slant ionospheric and tropospheric corrections are used to generate the correction at user station, which are usually interpolated by using distance-based linear interpolation [21],

$$T_{u,k} = \frac{\sum_{i=1}^{i=n} \frac{1}{D_i} T_{i,k}}{\sum_{i=1}^{i=n} \frac{1}{D_i}} \tag{29.7}$$

where, $T_{i,k}$ and $T_{u,k}$ are the tropospheric correction for epoch k, reference station i and user station u, D_i is the distance from reference station i to user station. The biased ionospheric correction derived from code and phase observations for epoch k at user station u ($I_{P,u,k}^b$ and $I_{L,u,k}^b$) at user station can be interpolated as,

$$I_{P,u,k}^b = \frac{\sum_{i=1}^{i=n} \frac{1}{D_i} I_{P,i,k}^b}{\sum_{i=1}^{i=n} \frac{1}{D_i}} = I_{u,k} + \frac{f_2^2}{f_1^2 - f_2^2} \left(b_{P_1}^s - b_{P_2}^s \right) + \frac{f_2^2}{f_1^2 - f_2^2} \frac{\sum_{i=1}^{i=n} \frac{1}{D_i} \left(b_{P_2,i}^r - b_{P_1,i}^r \right)}{\sum_{i=1}^{i=n} \frac{1}{D_i}} \tag{29.8}$$

$$I_{L,u,k}^b = \frac{\sum_{i=1}^{i=n} \frac{1}{D_i} I_{L,i,k}^b}{\sum_{i=1}^{i=n} \frac{1}{D_i}} = I_{u,k} - \frac{f_2^2}{f_1^2 - f_2^2} \left(b_{L_1}^s - b_{L_2}^s \right) - \frac{f_2^2}{f_1^2 - f_2^2} \frac{\sum_{i=1}^{i=n} \frac{1}{D_i} \left(b_{L_2,i}^r - b_{L_1,i}^r \right)}{\sum_{i=1}^{i=n} \frac{1}{D_i}} \tag{29.9}$$

where $I_{i,k}$ and $I_{u,k}$ are the ionospheric correction for epoch k, reference station i and user station u.

29.2.3 Fast Ambiguity Resolution at User Station Using Ionospheric and Tropospheric Constraint Equations

For a sparse reference network, the interpolated ionospheric and tropospheric corrections are not accurate enough for fast ambiguity resolution. Therefore, we still introduce the residual ionospheric delay δI and tropospheric delay δT for the observation equation at user station after applying satellite clock dt^s, interpolated tropospheric T_u, biased ionospheric corrections ($I_{P,u}^b$ and $I_{L,u}^b$), satellite code biases and FCBs. Then the observation equation at user station after correction is rewritten as

$$
\begin{cases}
P_1 - I^b_{P,u} - T_u + cdt^s + b^s_{P_3} = \rho + d_{orb} + cdt^r + B^r_{P_{1,u}} - B^s_{P_{1,u}} + \delta T + \delta I + \varepsilon_{P_1} \\
P_2 - \frac{f_1^2}{f_2^2} I^b_{P,u} - T_u + cdt^s + b^s_{P_3} = \rho + d_{orb} + cdt^r + B^r_{P_{2,u}} - B^s_{P_{2,u}} + \delta T + \frac{f_1^2}{f_2^2} \delta I + \varepsilon_{P_2} \\
L_1 + I^b_{L,u} - T_u + cdt^s + b^s_{L_3} = \rho + d_{orb} + cdt^r + B^r_{L_{1,u}} - B^s_{L_{1,u}} + \delta T - \delta I - \lambda_1 N_1 + \varepsilon_{L_1} \\
L_2 + \frac{f_1^2}{f_2^2} I^b_{L,u} - T_u + cdt^s + b^s_{L_3} = \rho + d_{orb} + cdt^r + B^r_{L_{2,u}} - B^s_{L_{2,u}} + \delta T - \frac{f_1^2}{f_2^2} \delta I - \lambda_2 N_2 + \varepsilon_{L_2}
\end{cases}
$$
$$(29.10)$$

where $B^r_{P_{*,u}}$, $B^r_{L_{*,u}}$ and $B^s_{P_{*,u}}$ and $B^s_{L_{*,u}}$ are mixed code biases and FCBs for receiver and satellite which are combination of biases at user and reference stations as follows

$$
\begin{cases}
B^r_{P_{1,u}} = b^r_{P_1,u} - \frac{f_2^2}{f_1^2 - f_2^2} \frac{\sum_{i=1}^{i=n} \frac{1}{D_i}\left(b^r_{P_2,i} - b^r_{P_1,i}\right)}{\sum_{i=1}^{i=n} \frac{1}{D_i}}, \quad B^s_{P_{1,u}} = \frac{f_2^2}{f_1^2 - f_2^2}\left[\left(b^s_{P_{1,u}} - b^s_{P_{2,u}}\right) - \frac{\sum_{i=1}^{i=n} \frac{1}{D_i}\left(b^s_{P_1,i} - b^s_{P_2,i}\right)}{\sum_{i=1}^{i=n} \frac{1}{D_i}}\right] \\[2em]
B^r_{P_{2u}} = b^r_{P_2,u} - \frac{f_1^2}{f_1^2 - f_2^2} \frac{\sum_{i=1}^{i=n} \frac{1}{D_i}\left(b^r_{P_2,i} - b^r_{P_1,i}\right)}{\sum_{i=1}^{i=n} \frac{1}{D_i}}, \quad B^s_{P_{2,u}} = \frac{f_1^2}{f_1^2 - f_2^2}\left[\left(b^s_{P_{1,u}} - b^s_{P_{2,u}}\right) - \frac{\sum_{i=1}^{i=n} \frac{1}{D_i}\left(b^s_{P_1,i} - b^s_{P_2,i}\right)}{\sum_{i=1}^{i=n} \frac{1}{D_i}}\right] \\[2em]
B^r_{L_{1,u}} = b^r_{L_1,u} + \frac{f_2^2}{f_1^2 - f_2^2} \frac{\sum_{i=1}^{i=n} \frac{1}{D_i}\left(b^r_{L_2,i} - b^r_{L_1,i}\right)}{\sum_{i=1}^{i=n} \frac{1}{D_i}}, \quad B^s_{L_{1,u}} = \frac{f_2^2}{f_1^2 - f_2^2}\left[\left(b^s_{L_{1,u}} - b^s_{L_2}\right) - \frac{\sum_{i=1}^{i=n} \frac{1}{D_i}\left(b^s_{L_1,i} - b^s_{L_2,i}\right)}{\sum_{i=1}^{i=n} \frac{1}{D_i}}\right] \\[2em]
B^r_{L_{2,u}} = b^r_{L_2,u} + \frac{f_1^2}{f_1^2 - f_2^2} \frac{\sum_{i=1}^{i=n} \frac{1}{D_i}\left(b^r_{L_2,i} - b^r_{L_1,i}\right)}{\sum_{i=1}^{i=n} \frac{1}{D_i}}, \quad B^s_{L_{2,u}} = \frac{f_1^2}{f_1^2 - f_2^2}\left[\left(b^s_{L_{1,u}} - b^s_{L_{2,u}}\right) - \frac{\sum_{i=1}^{i=n} \frac{1}{D_i}\left(b^s_{L_1,i} - b^s_{L_2,i}\right)}{\sum_{i=1}^{i=n} \frac{1}{D_i}}\right]
\end{cases}
$$
$$(29.11)$$

As the code biases and FCBs for one satellite at user stations is the same value as those at the reference stations, namely $b^s_{P_{1,u}} = b^s_{P_{1,i}}$, $b^s_{P_{2,u}} = b^s_{P_{2,i}}$, $b^s_{L_{1,u}} = b^s_{L_{1,i}}$, $b^s_{L_{2,u}} = b^s_{L_{2,i}}$. Thus, these satellite biases at user station will be compensated with the biased interpolated ionospheric correction $I^b_u \cdot B^s_{P_{1,u}} = B^s_{P_{2,u}} = B^s_{L_{1,u}} = B^s_{L_{2,u}} = 0$. On the other hand, despite that the receiver bias at user station is different with those at the reference stations, the receiver biases on the estimated biased iono-spheric correction is the same to all visible satellites at the user station. Thus, it can be absorbed by user receiver code bias and FCBs ($B^r_{P_{1,u}}$, $B^r_{P_{2,u}}$, $B^r_{L_{1,u}}$ and $B^r_{L_{2,u}}$). Therefore, such systematic biases have no effect on ionospheric corrections and the ambiguity-fixing at the user stations.

Since the interpolated ionospheric and tropospheric corrections are available at the user station, but exists some errors caused by either spatial extent of reference network or different elevations for the same satellites, we can form the following constraint equation to fast ambiguity resolution

$$
\begin{cases}
\delta I_k = \delta I_{k,0} + \varepsilon_{\delta I_k}, \quad \varepsilon_{\delta I_k} \sim N\left(0, \sigma^2_{\delta I_k}\right) \\
\delta T_k = \delta T_{k,0} + \varepsilon_{\delta T_k}, \quad \varepsilon_{\delta T_k} \sim N\left(0, \sigma^2_{\delta T_k}\right)
\end{cases}
$$
$$(29.12)$$

where $\delta I_{k,0}$ and $\delta T_{k,0}$ are the deterministic errors of interpolated ionospheric and tropospheric correction vector, which are generally given as zero. $\varepsilon_{\delta I_k}$ and $\varepsilon_{\delta T_k}$ are assumed to be random errors, the corresponding variances are $\sigma^2_{\delta I_k}$ and $\sigma^2_{\delta T_k}$. The ionospheric and tropospheric differences of the adjacent epochs can also use to form the constraint equation as follows

$$\begin{cases} \delta I_{r,k} - \delta I_{r,k-1} = w_{\delta I_k}, & w_{\delta I_k} \sim N\left(0, \sigma^2_{w_{\delta I_k}}\right) \\ \delta T_k - \delta T_{k-1} = w_{\delta T_k}, & w_{\delta T_k} \sim N\left(0, \sigma^2_{w_{\delta T_k}}\right) \end{cases} \tag{29.13}$$

where k is the current epoch; $k-1$ is the previous epoch; w_{I_k} and w_{T_k} are the differences of ionospheric and zenith tropospheric correction errors from previous epoch to current epoch; $\sigma^2_{w_{\delta I_k}}$ and $\sigma^2_{w_{\delta T_k}}$ are the variance of $w_{\delta I_k}$ and $w_{\delta T_k}$. The variances of Eqs. (29.12) and (29.13) must reflect the actual accuracies of the interpolated ionospheric and tropospheric corrections. If the variance is much smaller than its actual accuracy, it will result in the estimated ambiguities with considerable biases. Conversely, if the variance is much larger than its actual accuracy, it will cause constraint equation ineffective for improving the AR efficiency.

The variances of the interpolated ionospheric and tropospheric corrections can be properly estimated with the observations of a reference network using the following method. Firstly, we choose one station as simulated user station from n stations of a reference network, and interpolate the biased ionospheric correction for the user station using the remaining n-1 stations, then compute the difference between the estimated and interpolated ionospheric corrections as

$$\delta I_{r,k} = I^b_{r,k} - \frac{\sum_{i \in S} \frac{1}{D_{ri}} I^b_{i,k}}{\sum_{i \in S} \frac{1}{D_{ri}}}, \quad S = 1, 2, \ldots r - 1, r + 1, \ldots n \tag{29.14}$$

where r stands for the simulated user station, $I_{r,k}$ and $I_{i,k}$ are estimated ionospheric correction vector at simulated user station and the other $n-1$ stations. $\delta I_{r,k}$ is the difference between the estimated and interpolated ionospheric corrections at simulated user stations. Secondly, the variances $\sigma^2_{\delta I_k}$ and $\sigma^2_{w_{\delta I_k}}$ are computed by considering the distance between the simulated user and other reference stations. To avoid an over-optimistic constraint variance, the maximum value of interpolated error for all observed satellite is used. The $\sigma^2_{\delta I_k}$ and $\sigma^2_{w_{\delta I_k}}$ are written as

$$\sigma^2_{I_k} = \frac{\sum_{i=1}^{i=n} \frac{1}{D_i} \max\left(\delta I_{i,k}\right)^2}{\sum_{i=1}^{i=n} \frac{1}{D_i}} \tag{29.15}$$

$$\sigma^2_{w_{I,k,k-1}} = \left(\frac{\sum_{i=1}^{i=n} \frac{1}{D_i} \max\left(\delta I_{i,k} - \delta I_{i,k-1}\right)^2}{\sum_{i=1}^{i=n} \frac{1}{D_i}}\right) \tag{29.16}$$

In order to obtain confident variance estimates, we take the mean of latest m epochs estimates as,

$$\sigma_{I_k}^2 = \frac{\sum_{j=k-m+1}^{k} \sigma_{\delta I_j}^2}{m} \tag{29.17}$$

$$\sigma_{w_{I,k}}^2 = \frac{\sum_{j=k-m+1}^{k} \sigma_{w_{\delta I,j}}^2}{m} \tag{29.18}$$

The window length m should be reasonable chosen, because if it is too long, the computed constraint variance will be smooth to describe the detail of observation environment; while if it is too short, the estimate will be unstable. In our study, we take $m = 8$ for 15 s data interval. For the variance of tropospheric corrections, we can be estimated with the same way as ionospheric corrections.

The constraint level is reflected through the variance of the pseudo-observations, which is estimated with the reference network. The estimated variance is usually large in the sparse network, and small in a dense network, hence our proposed method can adapt any scale of reference network. Moreover, L1 and L2 observation equations are directly used to solve the L1 and L2 ambiguities and the LAMBDA method [22] is used to fix integer ambiguity.

29.3 Experiments and Results

In order to demonstrate the performance of the proposed methodology, two test networks of different spatial extent have been analyzed, called the network with medium inter-station distances and the network with long inter-station distances. The test networks were constructed by using several GPS stations of USA Continuously Operating Reference Stations (CORS) (Figs. 29.2, 29.8). Stations P505, P480, P510 and P510 constitute the medium reference network with inter-station distances of 41.4–65.3 km. 10 Stations located inside this network were chosen as a simulated user receiver with average distances to the reference stations of 36.4, 56.2, 28.6 and 60.3 km, respectively. The observation sampling interval is 15 s. The large network consists of stations SG04, SG10, SG46 and SG48 with inter-station distances of 65.2–114.7 km. And the stations SG01, SG42 and SG47 were simulated as user receivers with average distances to the reference stations of 84.5, 56.6, 62.9 and 80.8 km, respectively. The observation interval is also 15 s. The medium network was designed in such a way that it closely reflects the geometry and size of current CORS with an average station separation of 50 km. The elevation cut-off angle is 10°. The LAMBDA method is applied to conduct ambiguity resolution. Both ratio test and success rate are applied to validate the ambiguities [23]. The ratio threshold value is 2 and the success probability applied is 0.99 [24] (Fig. 29.1).
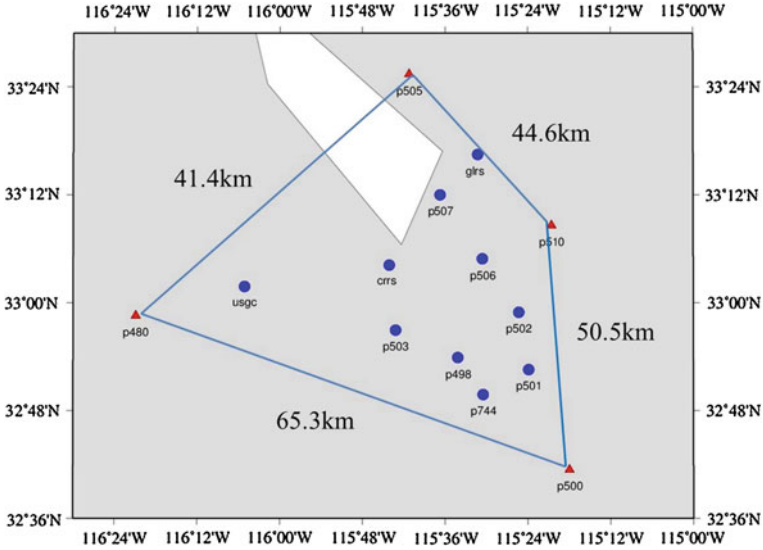
Fig. 29.1 Medium reference network, the *red triangle*—reference network, *blue circle*—user stations
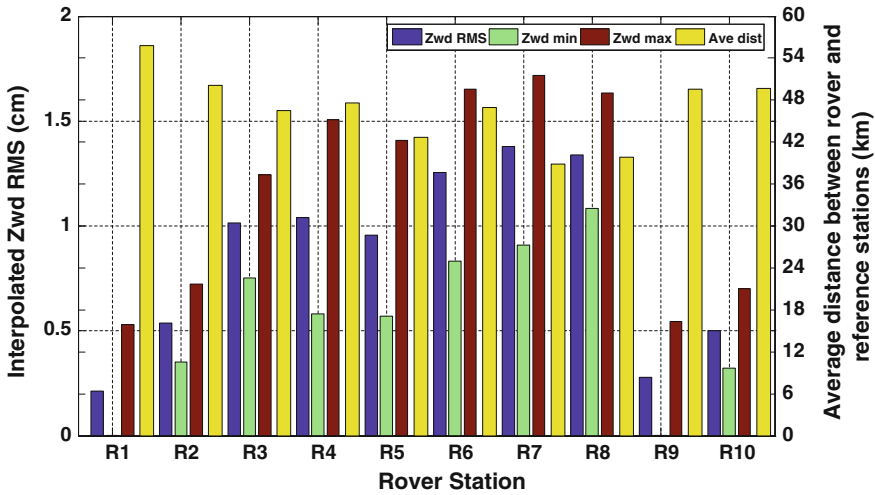

Fig. 29.2 Interpolated ZWD statistics compared to estimated ZWD at 10 user stations

The orbit and clock corrections are generated using the predicted orbits with initial condition fitted by using IGR orbits with 42 h arc length [25] and real-time estimated clocks [26]. The satellite FCBs are computed from a set of regional stations within USA in order to have a better fit to the region [13]. We process the

GPS data at the user stations in PPP mode and fix the integer ambiguities. Two PPP AR schemes are implemented for the purpose of comparison. Scheme 1 uses the traditional PPP AR mode which forms L3 observables of carrier-phases and pseudo-ranges while the tropospheric delay is estimated together with the position and ambiguity parameters. Scheme 2 uses the PPP AR mode augmented with regional network using our proposed method. The simulated user station is also processed as a reference station in advance in order to obtain the ionospheric and tropospheric delays for assessing the interpolated corrections from the other reference stations. The PPP ambiguity fixing at user station use interpolated ionospheric and tropospheric corrections.

29.3.1 Medium Network

Taking the zero-differenced (ZD) ionospheric and tropospheric delays retrieved at the four reference stations, we interpolate the ionospheric and tropospheric corrections for the user stations epoch by epoch, and present statistic results in Figs. 29.2 and 29.3 for tropospheric and ionospheric corrections, respectively. Figure 29.2 shows several interpolated ZWD statistics of 10 user stations. The ZWD RMSs for user stations are from 0.2 to 1.4 cm, which is essentially reflects the average spatial extent between user station and reference stations. Figure 29.3 shows the RMSs statistics of interpolated ionospheric corrections, which are derived from the differences between the estimated and interpolated corrections, and the differences for the user station crrs are shown in left panel of Fig. 29.4. The variances of interpolated slant ionospheric corrections achieve 2.1–5.2 cm in Fig. 29.3, which are significantly larger than those of ZWD and its variation is not very consistent with average spatial extent between user station and reference stations as ZWD. From right panel of Fig. 29.4 we can see that $\sigma_{\delta I_k}$ show in red envelops most of interpolated ionospheric errors, which is big enough to avoid bias in the AR while constraint with $2\sigma_{\delta I_k}$ shown in green is obviously loose compared to the actual interpolated correction error. Besides, $\sigma_{\delta I_k}$ is much larger than interpolated ionospheric errors, especially during the UTC 16:00 to 24:00 when is the day time at that region and the ionosphere activities are relatively strong. This result shows that the proper constraint variance can be determined when the ionosphere is quiet. When the ionosphere is active, bigger constraint variance would be determined, which would affect AR efficiency but not cause bias in AR model.

The TTFS of all 10 user stations in medium network is computed and counted. A typical cumulative distribution of PPP TTFS with 10 rover stations is shown in Fig. 29.5. The probabilities of TTFS are 7.0, 88.6, 95.1, and 95.5 % for the observation time with 15, 30, 45 min and 1 h, respectively. The average TTFS is 21.9 min. The results show that the longer the observation time is used the higher the TTFS can be achieved. As the longer the observation time used in float PPP
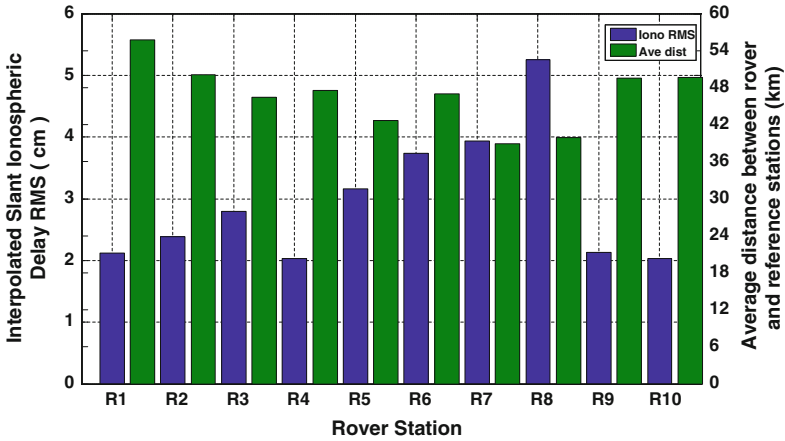
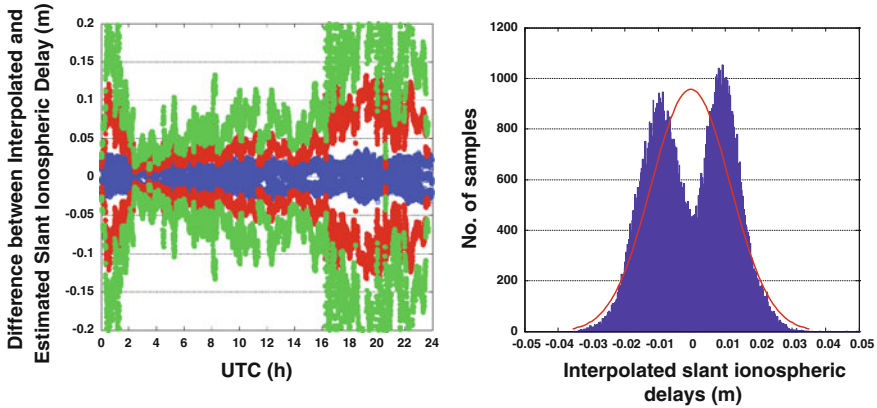**Fig. 29.3** Interpolated ionospheric statistics compared to estimated ionospheric delay at 10 user stations

Fig. 29.4 Difference between interpolated and estimated ZD ionospheric delays over 24 h at user station crrs (*blue circle in left panel*). The *red circle* presents σ_{I_k} while the *green circle* presents $2\sigma_{I_k}$. The *right panel* shows the distribution of difference between interpolated and estimated ZD ionospheric delays over 24 h

solution the more accurate the float ambiguity, and so the more reliably integer ambiguity can be fixed. The TTFS probability is improved significantly when the length of the observation time increases from 15 to 30 min. In comparison, only a small improvement is found when the observation time lengthens are increased to 45 min and 1 h. With regional augmented tropospheric and ionospheric
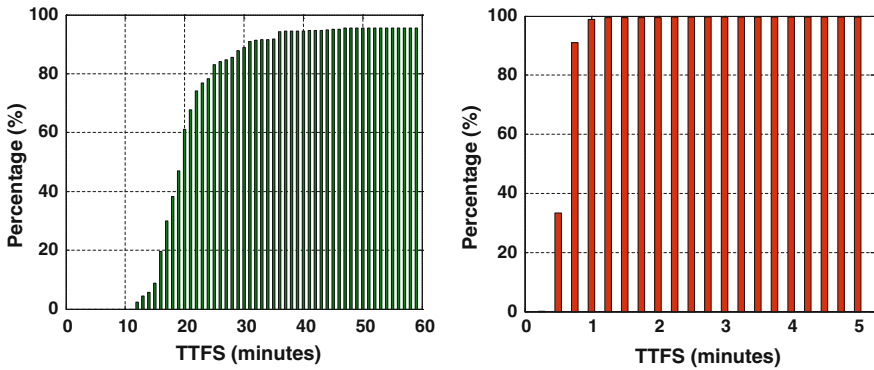
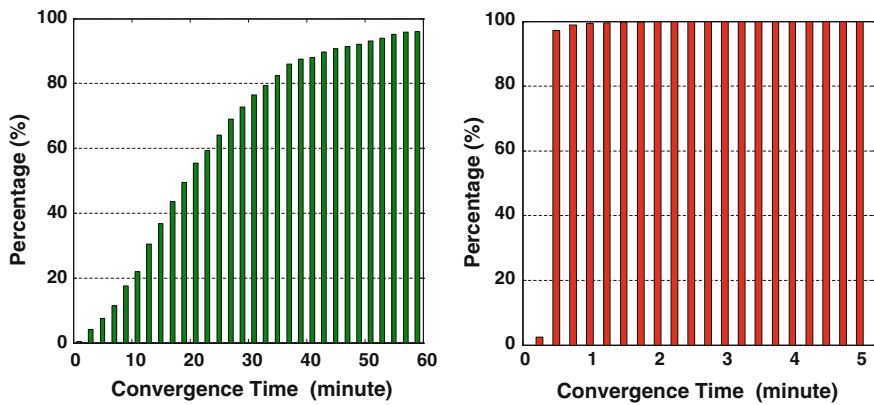**Fig. 29.5**   Cumulative distribution of TTFS (scheme 1 vs. scheme 2)

Fig. 29.6   Cumulative distribution of convergence time (scheme 1 vs. scheme 2)

corrections, the probability of TTFS can achieve 93.5 % only using 1 min observations. It can be seen that the scheme 1 requires 19.5 min to fix the L1 and L2 ambiguities while the scheme 2 successfully fixed ambiguity within 1 min. For ambiguity-float kinematic PPP results, as shown in Fig. 29.6, the average convergence time is 22.5 min for the scheme 1 while only 30.8 s for the scheme 2. Here, the 'convergence' means a 3D positioning error achieves less than 10 cm (Fig. 29.6).
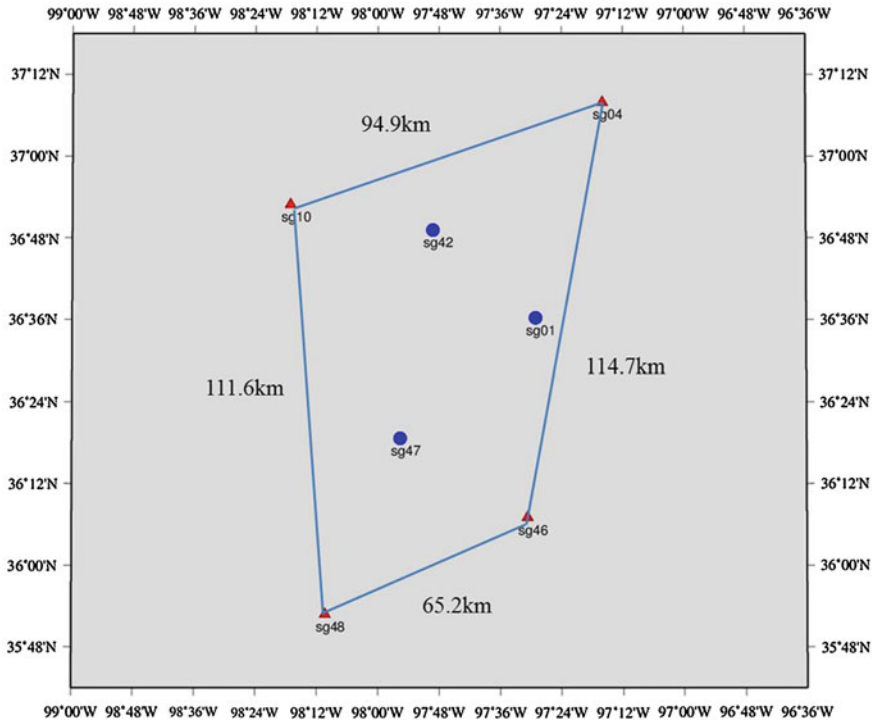
Fig. 29.7 Large regional network distribution, the *red triangle*—reference network, *blue circle*—user stations

Table 29.1 Interpolated atmospheric correction accuracy with large network

User station	Ave dist (km)	Interpo. ZWD RMS (cm)	Interpo. Iono RMS (cm)
Sg01	69.6	1.8	5.7
Sg42	73.5	2.0	6.8
Sg47	71.9	2.1	7.3

29.3.2 Large Network

Table 29.1 shows the accuracies of interpolated ionospheric and tropospheric corrections for the large network with average distance of about 70 km as shown in Fig. 29.7. It can be seen that both of the interpolated ZWD and ionospheric correction error become bigger compared to the RMS of interpolated ZWD errors using a medium network. However, the RMS of interpolated ionospheric error achieves 5.7–7.3 cm centimeters, which are significant and cannot be neglected. Figure 29.8 shows the difference between the interpolated and estimated ZD ionospheric delays over an 8-h period when the ionosphere is quiet and the
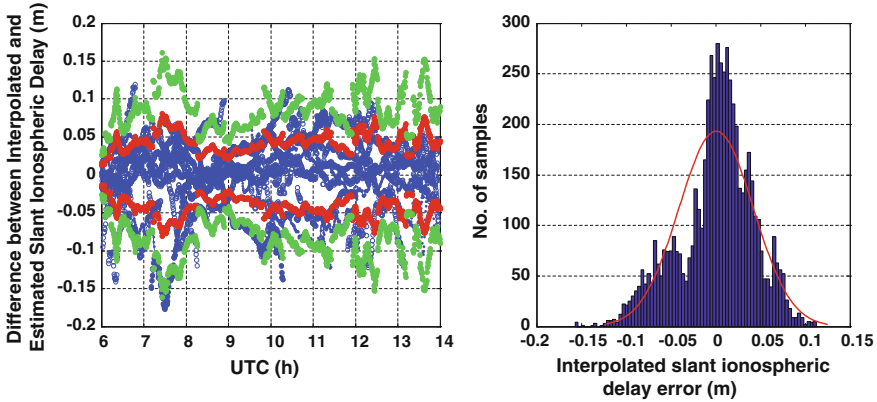
Fig. 29.8 Difference between interpolated and estimated ZD ionospheric delays over 8 h at rover station sg01 (*blue circle in left panel*). The *red circle* presents σ_{I_k} while the *green circle* presents $2\sigma_{I_k}$. The *right panel* shows the distribution of difference between interpolated and estimated ZD ionospheric delays
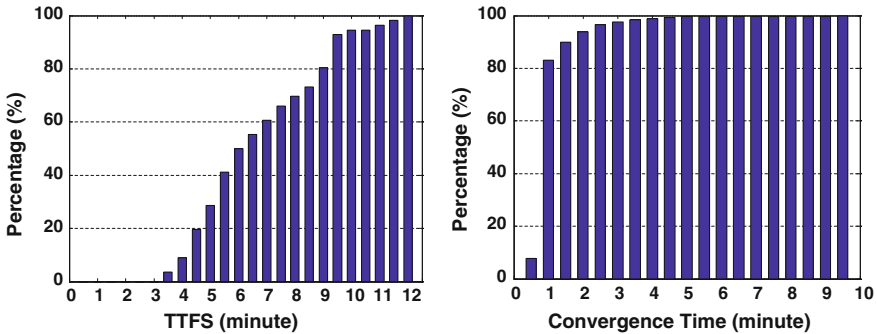

Fig. 29.9 Cumulative distribution of TTFS and convergence time of large network (scheme 2)

ionospheric constraint variance. For the large network, it can be seen that σ_{I_k} shown in red only envelops about 60 % of the interpolated ionospheric errors. That means this constraint variance is still optimistic for 40 % of ionospheric errors. If we use $2\sigma_{I_k}$ as the constraint variance, more than 90 % of ionospheric errors can be enveloped. In practice, a conservative constraint variance should be given to avoid bias in ambiguities. Thus, it's better to use $2\sigma_{I_k}$ as the constraint variance for large networks.

For large networks, a typical cumulative distribution of PPP TTFS and convergence time with 3 user stations is shown in Fig. 29.9. Both of TTFS and convergence time increase compared to the results of medium network, but still have significant improvement. The TTFS probability achieves 28.6 and 94.6 % when the observation time is 5 and 10 min. The average TTFS is 6.9 min. For

ambiguity-float kinematic PPP, the percentage of convergence time achieves 83.3, 93.8 and 99.6 % for the observation time with 1, 2 and 5 min, respectively, and on average the convergence time is 71.9 s.

29.4 Conclusions

We have developed a new strategy to augment PPP by mitigating the spatial errors by using ionospheric and tropospheric corrections derived from a sparse regional reference network, so that fast ambiguity fixing can be achieved for users within the network coverage. Since the ionospheric and tropospheric correction errors vary with the spatial geometry of the reference network, the atmospheric constraint variance is adaptively determined for different networks in real time. The method has been validated with two regional networks. From the experimental results, the ZWD correction errors are less than 1 cm on average while the ionospheric correction error is about 3 cm for medium size networks. Thus, the performance of PPP capable of fast ambiguity resolution can be comparable to NRTK. Despite both interpolated ZWD and ionospheric correction errors increase for large networks, the average convergence time and TTFS can achieve 71.9 s and 6.9 min, respectively. With this proposed method, it can extend the inter-station distances to more than 100 km for current reference RTK networks but still can achieve centimeter level position solutions within 10 min.

References

1. Kouba J (2009) A guide to using international GNSS service (IGS) products. http://igscb.jpl. nasa.gov/components/usage.html
2. Dixon K (2006) StarFire TM: a global SBAS for sub decimetre precise point positioning. In: Proceedings of ION GNSS 2006, Institute of Navigation, Fort Worth, Texas, pp 2286–2296
3. Dousa J (2010) The impact of errors in predicted GPS orbits on zenith troposphere delay estimation. GPS Solutions 14:229–239
4. Shi C, Lou Y, Zhang H, Zhao Q, Geng J, Wang R, Fang R, Liu J (2010) Estimating seismic displacement of the Mw8.0 wenchuan earthquake from high-rate GPS observations. Adv Space Res 46(2):228–235
5. Ge M, Gendt G, Rothacher M, Shi C, Liu J (2008) Resolution of GPS carrier-phase ambiguities in precise point positioning (PPP) with daily observations. J Geodesy 82(7):389–399
6. Laurichesse D, Mercier F, Berthias JP, Broca P, Cerri L (2009) Integer ambiguity resolution on un differenced GPS phase measurements and its application to PPP and satellite precise orbit determination. Navigation 56(2):135–149
7. Collins P (2008) Isolating and estimating un-differenced GPS integer ambiguities. In: Proceedings of ION national technical meeting, San Diego, US, pp 720–732
8. Li B, Feng Y, Shen Y, Wang C (2010) Geometry-specified troposphere decorrelation for subcentimeter real-time kinematic solutions over long baselines. J Geophys Res 115:B11404
9. Dodson A, Shardlow P, Hubbard L, Elgered G, Jarlemark P (1996) Wet tropospheric effects on precise relative GPS height determination. J Geod 70:188–202. doi:10.1007/BF00873700

10. Tralli D, Lichten S (1990) Stochastic estimation of tropospheric path delays in global positioning system geodetic measurements. Bull Geodesy 64:127–159. doi:10.1007/BF02520642
11. Shi J (2012) Precise point positioning integer ambiguity resolution with decoupled clocks. PhD thesis, Department of Geomatics Engineering University of Calgary, UCGE Report 20367
12. Ge M, Zou X, Dick G, Jiang W, Wickert J, Liu J (2010) An alternative Network RTK approach based on un differenced observation corrections ION GNSS, Portland, Oregon
13. Li X, Zhang X, Ge X (2011) Regional reference network augmented precise point positioning for instantaneous ambiguity resolution. J Geodesy 85:151–158
14. Teunissen P (1997) The geometry-free GPS ambiguity search space with a weighted ionosphere. J Geodesy 71(6):370–383
15. Odijk D (2000) Weighting ionospheric corrections to improve fast GPS positioning over medium distances. In: Proceedings of ION GPS-2000, Institute of Navigation, Alexandria, pp 1113–1123
16. Horemuz M, Sjoberg LE (2002) Rapid GPS ambiguity resolution for short and long baselines. J Geodesy 76:381–391
17. Wielgosz P, Kashani I, Grejner-Brzezinska D (2005) Analysis of long-range network RTK during severe ionospheric storm. J Geodesy 79(9):524531
18. Wielgosz P (2011) Quality assessment of GPS rapid static positioning with weighted ionospheric parameters in generalized least squares. GPS Solutions 15:89–99
19. Li Y, Shen Y (2011) INS aided ambiguity resolution for GPS/INS integrated kinematic positioning, ION GNSS
20. Li X (2012) Improving real-time PPP ambiguity resolution with ionospheric characteristic consideration. In: Proceedings of ION GPS 2012 Nashville TN Sept 17–21
21. Gao Y, Li Z, McLellan JF (1997) Carrier phase based regional area differential GPS for decimeter-level positioning and navigation. In: Proceedings of 10th international technical meeting of the Satellite Division of US Institute of Navigation, Kansas, City, pp 1305–1313, Sept 16–19
22. Li B, Verhagen S, Teunissen PJG (2013) GNSS integer ambiguity estimation and evaluation: LAMBDA and Ps-LAMBDA. In: Proceedings of China satellite navigation conference (CSNC) 2013, lecture notes in electrical engineering, vol 24. Wuhan, pp 291–301
23. Verhagen S (2005) On the reliability of integer ambiguity resolution. Navigation 52(2):99–110
24. Li P, Zhang X (2013) Integrating GPS and GLONASS to accelerate convergence and initialization times of precise point positioning. GPS Solutions 15:315–324
25. Choi K, Ray J, Griffiths J, Bae T (2012) Evaluation of GPS orbit prediction strategies for the IGS Ultra-rapid products. GPS Solutions. doi:10.1007/s10291-012-0288-2
26. Hauschild A, Montenbruck O (2009) Kalman-filter-based GPS clock estimation for near real-time positioning. GPS Solutions 13:173–182